Geometrically frustrated triangular lattice system Na_xVO_2: superparamagnetism in $x = 1$ and trimerization in $x \approx 0.7$

2008 J. Phys.: Condens. Matter 20 145205

(http://iopscience.iop.org/0953-8984/20/14/145205)

J. Phys.: Condens. Matter **20** (2008) 145205 (8pp) doi:10.1088/0953-8984/20/14/145205

Geometrically frustrated triangular lattice system Na_xVO_2: superparamagnetism in $x = 1$ and trimerization in $x \approx 0.7$

Masashige Onoda

Institute of Physics, University of Tsukuba, Tennodai, Tsukuba 305-8571, Japan

E-mail: onoda@sakura.cc.tsukuba.ac.jp

Received 13 December 2007, in final form 19 February 2008
Published 18 March 2008
Online at stacks.iop.org/JPhysCM/20/145205

Abstract

The structural and electronic properties of the triangular lattice system Na_xVO_2 with $x = 1$ and ≈ 0.7 are explored by x-ray powder diffraction and through transport and magnetic measurements. For $x = 1$, the structure at 293 K is modelled by three oxygen layers with an octahedral oxygen environment for Na. This composition, which is classified as being an insulator phase, exhibits superparamagnetism below the transition temperature $T_{ms} \simeq 98$ K to a tripled unit cell. Above T_{ms}, the temperature dependence of magnetic susceptibility is understood in terms of the *pseudotrimer* model, using the exchange coupling constant determined from a high-temperature series expansion. This model is also applied to the paramagnetic phase for $LiVO_2$, which indicates spin-singlet trimerization at $T_{c1} \approx 500$ K on heating and $T_{c2} \approx 440$ K on cooling. The compound with $x \approx 0.7$ basically has a two-layer structure with a prismatic oxygen surrounding Na and it may exhibit a first-order spin-$\frac{1}{2}$ trimerization at $T_{c1} \approx 360$ K and $T_{c2} \approx 290$ K.

1. Introduction

Since the proposal of a resonating-valence-bond theory or a spin–liquid ground state for a triangular lattice system with Heisenberg interaction, geometrically frustrated spin systems have received a great deal of attention [1, 2]. The frustration effects cause the temperature of the transition to a possible ordered phase to be reduced significantly. Structural phase transitions to lower symmetry sometimes occur due to a gain in orbital and magnetic energies on lifting the degeneracy as, for example, found in $LiVO_2$ [3–6]. The recent discovery of superconductivity in $Na_{0.3}CoO_2{\cdot}1.3H_2O$ [7] as well as the possible application to thermoelectric devices in the parent compound Na_xCoO_2 [8] has accelerated investigations of this system. It has also been postulated that in $NiGa_2S_4$, a spin-disordered state is stabilized by geometrical frustration [9].

A typical triangular lattice ternary oxide has a chemical formula of MTO_2, where M is an alkaline metal and T is a transition metal [10, 11]. The structure is basically described in terms of TO_6 octahedra which are joined by sharing edges to form a two-dimensional triangular lattice. The M atoms are located between these lattices. MTO_2 and its nonstoichiometric series M_xTO_2 are classified according to the type of oxygen coordination for M, which is either octahedral (O) or prismatic (P), and to the number of oxygen layers for a unit cell, Generally, the stoichiometric MTO_2 phase has a three-layer structure, which is expressed as O3 or P3. The O3 structure corresponds to an ordered rock-salt type.

$LiVO_2$ basically has the O3 structure and exhibits a spin-singlet trimerization at $T_{c1} \approx 500$ K on heating and $T_{c2} \approx 440$ K on cooling [3–6]. This was considered to be due to the *spin-lattice interaction* in the antiferromagnetically coupled spin-1 triangular system. The trimerized phase corresponds to a two-dimensionally ordered state and the structural correlation between the basal planes is incoherent. In addition, the small doping of spin-$\frac{3}{2}$ for this system leads to spin-$\frac{1}{2}$ per three V ions as a ground state [6]. The trimerization has been discussed from the viewpoint of orbital ordering in which a three-orbital sublattice is formed in the pseudocubic (1 1 1) planes of V ions [12]. This picture partly supports our model, but it is not clear whether or not the doping effect and the incoherent nature of the structure are explained.

This paper considers the Na_xVO_2 system with $x = 1$ and ≈ 0.7. Previous reports for these compounds are summarized as follows [13]: $NaVO_2$ is orthorhombic at room temperature with lattice constants of $a = 9.099$, $b = 7.163$ and $c =$

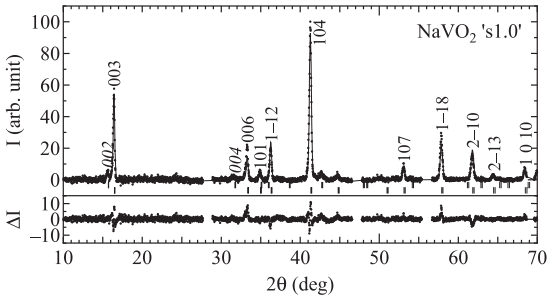

Figure 1. The x-ray powder diffraction pattern of 's1.0' prepared from nominal composition $NaVO_2$ with Cu Kα radiation and a rapid scan condition at 293 K. The result in terms of Rietveld refinement is indicated by the full curve in the top panel and the difference between the observed and calculated intensities is plotted in the bottom panel. The regular and italic letters show the indices for $NaVO_2$ and $Na_{0.7}VO_2$, respectively.

5.386 Å, while at 473 K, it is trigonal with $a = 2.995$ and $c = 16.29$ Å. At 368–388 K, a semireversible crystallographic transition occurs. In addition, the stoichiometric compound reacts instantly with air to generate a composition close to $Na_{0.6}VO_2$ which is estimated through an electrochemical oxidation. The atomic parameters for this system have not been published. The present work will provide results significantly different from the previous ones and lead to more definite pictures for Na_xVO_2 through careful analyses in spite of the specimen with a second phase. Details regarding the sample preparation and the measurements are given in section 2. The structural models of Na_xVO_2 with $x = 1$ and $\approx$0.7 considered on the basis of the x-ray powder diffraction are presented in sections 3.1.1 and 3.1.2, respectively; the transport properties revealed through measurements of the electrical resistivity and thermoelectric power are described in section 3.2, and magnetic properties for $x = 1$ and $\approx$0.7 clarified based on the magnetization measurements are given in sections 3.3.1 and 3.3.2, respectively. Section 4 is devoted to conclusions.

2. Experiments

Polycrystalline specimens of nominal compositions Na_xVO_2 ($x = 1$ and $\approx$0.7), hereafter referred to as 's1.0' and 's0.7', were prepared by the solid-state reaction method using a x:1 molar mixture of Na_2CO_3 (99% purity) and V_2O_5 (99.99% purity) in an N_2/H_2 gas flow at 893 and 908 K, respectively. Unfortunately this preparation method does not provide single-phase specimens, as will be described in section 3.1. However, it is considered to be the best way in solid-state reactions using various reaction temperatures and several different starting materials.

Inductively coupled plasma-optical emission spectroscopy (ICP) was performed using a Nippon Jarrell-Ash ICAP-575 spectrometer. An x-ray powder diffraction pattern was taken with Cu Kα radiation at 293 and 96 K using a Rigaku RAD-IIC diffractometer. In order to minimize the reaction of the specimens with air, all of the x-ray measurements were carried out in a vacuum. For 's1.0', rapid scan measurements were applied. The four-terminal electrical resistivity and the thermoelectric power were measured with the dc method at temperatures between 80 and 300 K. The magnetization measurements were performed at temperatures between 4.2 and 900 K by the Faraday method with a field of up to 1 T. The magnetic susceptibility was deduced from the linear part of the magnetization-field (M–H) curve with a decreasing field.

Table 1. Atomic coordinates and isotropic thermal parameters U_{iso} of $NaVO_2$ at 293 K.

Atom	Site	Occupancy	x	y	z	U_{iso} (Å^2)
V	3a	1	0	0	0	0.0215(19)
Na	3b	1	0	0	$\frac{1}{2}$	0.008(3)
O	6c	1	$\frac{2}{3}$	$\frac{1}{3}$	0.0650(4)	0.017(3)

3. Results and discussions

3.1. Structural models

3.1.1. $NaVO_2$. ICP analyses for 's1.0' and 's0.7' indicate that the specimens have Na concentrations of 1.06(1) and 0.70(1) per V ion, which is nearly consistent with the nominal compositions. Figure 1 indicates the x-ray powder diffraction pattern of 's1.0' at 293 K with a rapid scan condition, where the reflections from the Si standard are removed. Almost all of the diffraction peaks are indexed with trigonal and hexagonal phases; the former main phase, called 's1.0a', has dimensions in a hexagonal basis of $a = 2.9980(1)$ and $c = 16.106(1)$ Å, and the latter 's1.0b' phase has values similar to those of the main phase of 's0.7', as will be described below. It is confirmed that exposure of 's1.0' to air increases the relative intensity of the 's1.0b' phase. Two undefined peaks exist at $2\theta \simeq 42.8°$ and 44.9°. Note that $LiVO_2$ provides a diffuse reflection with wavevector $(\frac{h}{3}\ \frac{h}{3}\ 0)$ below the spin-singlet trimerization temperature [3]. For 's1.0a' at 293 K, these superlattice reflections do not exist, while at 96 K, a significant peak appears (not shown).

On the basis of the Rietveld analysis [14] with the assumption of space groups $R\bar{3}m$ and $P6_3/mmc$ for the 's1.0a' and 's1.0b' phases, respectively, the structure of the 's1.0a' phase is modelled taking account of the atomic parameters for unmodulated crystals of $LiVO_2$ in the paramagnetic state [3]. Here the atomic parameters for the 's1.0b' phase are the same as those of $Na_{0.7}VO_2$ as will be presented in the analysis for 's0.7'. The atomic parameters for the structural model of the 's1.0a' phase or $NaVO_2$ are listed in table 1. The relative amount of this phase is about 97%. Here the discrepancy factors are $R_p = \sum|Y_o - Y_c|/\sum|Y_o| = 8.6\%$ and $R_{wp} = [\sum w(Y_o - Y_c)^2/\sum wY_o^2]^{1/2} = 10.7\%$, where Y_o and Y_c are the observed and calculated intensities of the pattern, respectively. Clinographic views of the structural model of $NaVO_2$ are shown in figure 2.

The V ions in $NaVO_2$ are surrounded octahedrally with a V–O distance of 2.023(4) Å. As shown in figures 2(a) and (b), there exist three triangular lattice layers of VO_2 linked by edge-shared VO_6 octahedra in the unit cell. The Na atoms located between the layers are surrounded octahedrally with Na–O bonds of 2.382(5) Å, which agrees well with the value

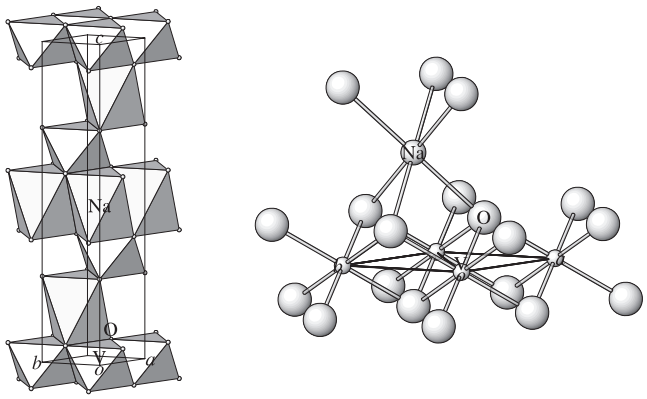

Figure 2. Clinographic views for the structural model of $NaVO_2$ at 293 K in terms of (a) the polyhedral and (b) bond schemes ($c/3$ unit).

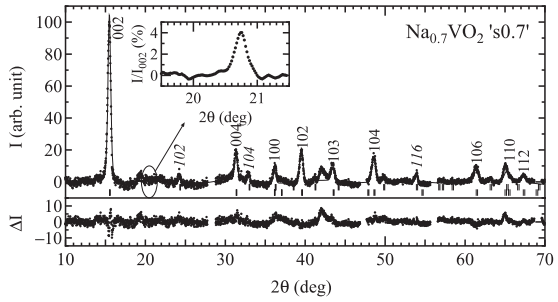

Figure 3. The x-ray powder diffraction pattern of 's0.7' prepared from the nominal composition $Na_{0.7}VO_2$ with Cu Kα radiation at 293 K. The result in terms of Rietveld refinement is indicated by the full curve in the top panel and the difference between the observed and calculated intensities is plotted in the bottom panel. The regular and italic letters show the indices for $Na_{0.7}VO_2$ and V_2O_3, respectively. The inset shows the magnified profile at around the superlattice point ($\frac{1}{3}$ $\frac{1}{3}$ 0) normalized by the reflection intensity I_{002} for (0 0 2).

for a six-coordinated Na ion [15]. Therefore the structure of $NaVO_2$ is O3 type. The isotropic thermal parameters U_{iso} may be in a normal range for all the atoms. The V valence calculated from the bond-lengths–bond-strengths relation [16] is 2.89(4), which nearly agrees with that from the chemical formula, assuming the full occupancy of O ions.

3.1.2. $Na_{0.7}VO_2$. The powder diffraction pattern of 's0.7' at 293 K is shown in figure 3, which approximately consists of hexagonal 's0.7a' and trigonal 's0.7b' phases; the 's0.7a' phase has a pattern similar to that of 's1.0b' with cell dimensions of $a = 2.8668(4)$ and $c = 11.399(1)$ Å, and the 's0.7b' phase is V_2O_3 [17]. One undefined peak is seen at $2\theta \simeq 42.1°$.

From the Rietveld analysis for 's0.7' with space groups $P6_3/mmc$ and $R\bar{3}c$ for the 's0.7a' and 's0.7b' phases, respectively, the structural model of the 's0.7a' phase is constructed by reference to the atomic parameters for unmodulated crystals of $Na_{0.58}CoO_2$ [18], where the atomic parameters for the 's0.7b' phase are the same as those of V_2O_3 reported previously [17]. The atomic parameters for the

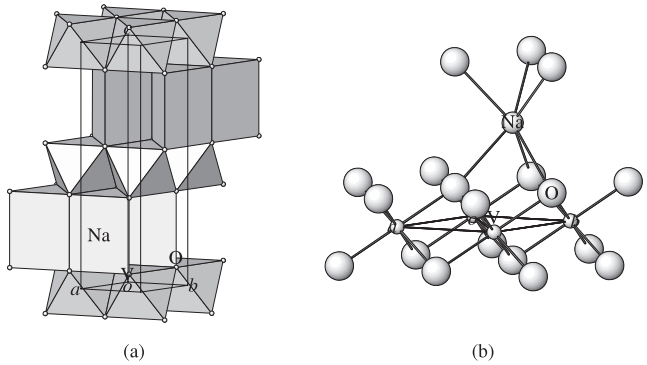

Figure 4. The clinographic views for the average structural model of $Na_{0.7}VO_2$ at 293 K in terms of (a) the polyhedral and (b) bond schemes ($c/2$ unit).

Table 2. Atomic coordinates and isotropic thermal parameters U_{iso} for the average structure of $Na_{0.7}VO_2$ at 293 K.

Atom	Site	Occupancy	x	y	z	U_{iso} (Å^2)
V	2a	1	0	0	0	0.015(3)
Na	2c	0.7	$\frac{1}{3}$	$\frac{2}{3}$	$\frac{1}{4}$	0.062(8)
O	4f	1	$\frac{2}{3}$	$\frac{1}{3}$	0.0955(19)	0.042(6)

structural model of the 's0.7a' phase or $Na_{0.7}VO_2$ are listed in table 2. Here the occupancy probability of Na is fixed at 0.7. It is noted that in $Na_{0.58}CoO_2$, the Na atoms are located not only in the 2c site but also in (0 0 $\frac{1}{4}$) of 2b [18]. The present Fourier synthesis indicates no peak at the 2b site. The relative amount of this phase is about 91% and the discrepancy factors are $R_p = 6.6\%$ and $R_{wp} = 8.4\%$. Figures 4(a) and (b) indicate the clinographic views of the structural model of $Na_{0.7}VO_2$.

In $Na_{0.7}VO_2$, the V ions have an octahedral coordination with V–O distance of 1.965(6) Å. Two triangular lattice layers of VO_2 linked by edge-shared VO_6 octahedra are formed in the unit cell. The partially occupied Na atoms have a trigonal prismatic environment with an Na–O distance of 2.438(9) Å, consistent with the value for six-coordinated Na ion [15]. Thus $Na_{0.7}VO_2$ has the P2 structure[1]. The large U_{iso} value for Na may be predominantly attributed to the significant oscillation of atoms due to the partial occupation. The V valence calculated from the bond-lengths–bond-strengths relation [16] is 3.46(7), which is close to the value expected from the chemical formula. Detailed measurements indicate that the superlattice reflection at around ($\frac{1}{3}$ $\frac{1}{3}$ 0) exists at 293 K as shown in the inset of figure 3. Therefore, the structural model evaluated above is of the average structure. In other words, significant displacements of V and/or Na ions in the ab-plane, such as in the trimerized V lattice in $LiVO_2$ [3–6], may be expected. Actually, this composition exhibits a first-order phase transition at temperatures between 290 and 360 K, as described in subsequent sections. It is known that the average model for the superlattice structure often gives large anisotropic displacement parameters [5], but it is difficult to clarify this property from the present data alone.

[1] The nominal compound $Na_{0.7}VO_2$ synthesized at a temperature slightly higher than the present condition is found to have the O3 structure.

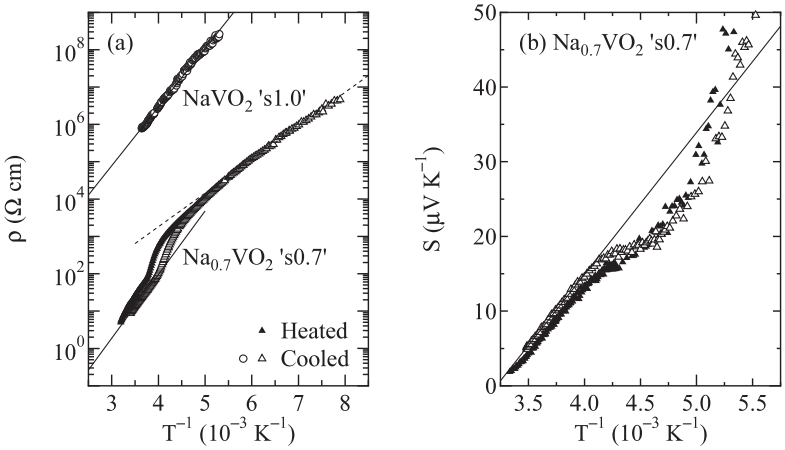

Figure 5. (a) The electrical resistivities against the inverse of temperature for 's1.0' and 's0.7' prepared from the nominal compositions $NaVO_2$ and $Na_{0.7}VO_2$, respectively. (b) The thermoelectric powers as a function of the inverse temperature for 's0.7'. Here, the lines in (a) and (b) denote fits to equations (1) and (2), respectively, with parameters given in the text.

The layered structures in the M_xTO_2 system sometimes exhibit a stacking fault [19], which causes complicated profiles. In order to know detailed structural properties of Na_xVO_2 with $x = 1$ and ≈ 0.7, further investigations of the single-phase specimens as well as of the single-crystalline ones are needed.

3.2. Transport properties

The electrical resistivities ρ against the inverse of temperature for 's1.0' and 's0.7' are shown in figure 5(a). The resistivity of 's1.0' is of the order 10^6 Ω cm at room temperature, indicating $NaVO_2$ to be an insulator basically due to the electron correlation, since the impurity phase of $Na_{0.7}VO_2$ has a significantly small resistivity as described below. For the temperature range measured, the empirical formula

$$\rho \propto \exp(E_\rho/T), \tag{1}$$

is applied with the apparent activation energy $E_\rho = 3.62(2) \times 10^3$ K as shown by the full line in figure 5(a). The resistivity for 's0.7' is significantly smaller than that for 's1.0' and it is of the order of 10^0 Ω cm, suggesting that $Na_{0.7}VO_2$ is like a semiconductor. Although this specimen has a minor phase of V_2O_3, the data do not show any trace of a metal–insulator transition of that compound. Thus, the result presented here may reflect the intrinsic nature of $Na_{0.7}VO_2$. On cooling from 300 K, the resistivity increases with $E_\rho = 3.92(1) \times 10^3$ K above 250 K as shown by the full line, and it does so more rapidly down to 200 K. At lower temperatures, it has $E_\rho = 2.07(1) \times 10^3$ K as indicated by the dotted line. For the heated process, this anomalous change of the resistivity shifts to higher temperature, indicating a first-order phase transition.

The temperature dependence of the thermoelectric power S for 's0.7' is shown in figure 5(b). For the temperature region measured, the thermoelectric power is positive, which indicates the carrier to be hole. On decreasing temperature from 300 to 250 K, the thermoelectric power increases gradually, and between 250 and 210 K, it exhibits a plateau, and at the lower temperatures, it increases rapidly. This anomalous change may correspond to that for the resistivity, although the thermal hysteresis of the thermoelectric power is less significant. The overall temperature dependence is like a semiconductor, although it is different from that expected in a simple wide band model. Applying the relation,

$$S = S_0 + E_S/T, \tag{2}$$

for the data above 250 K, a constant component and the apparent gap are obtained as $S_0 = -61.0(4)$ μV K^{-1} and $E_S = 220(1)$ K, respectively, as indicated by the full line in figure 5(b). The difference between E_ρ and E_S has often been observed in nonstoichiometric transition-metal oxide systems, that is, the ionic deficiency and/or randomness effects may produce a finite density of states at the Fermi level, which in some cases, gives a polaronic conduction or a strongly correlated behaviour at high temperatures and a variable-range hopping conduction at low temperatures [20, 21]. This may be the case for $Na_{0.7}VO_2$ with an Na deficiency.

3.3. Magnetic properties

3.3.1. $NaVO_2$. The temperature dependence of the inverse of magnetic susceptibility χ^{-1} for 's1.0' is shown in figure 6. On cooling from the high-temperature side, the susceptibility increases and exhibits a slight decrease at $T_{c1(c2)} \approx 380$ (330) K in the heated (cooled) processes, respectively. As will be found in section 3.3.2, this temperature range of the first-order transition roughly corresponds to that for 's0.7'. The decrease of susceptibility for 's1.0' is $\Delta\chi \approx 1.9 \times 10^{-5}$ emu mol^{-1}, which suggests that 's1.0b' or $Na_{0.7}VO_2$ gives rise to the suppression of susceptibility considering the results of structure analysis. In other words, $NaVO_2$ does *not* exhibit a spin-singlet transition for this temperature range. A kink of χ^{-1} appears at $T_{ms} \simeq 98$ K, below which the susceptibility has a significant temperature dependence. As shown in figures 7(a) and (b), the M–H curves have upward (downward) curvatures for positive (negative) fields at low temperatures and the susceptibility estimated from the linear part at low fields becomes constant below 12 K.

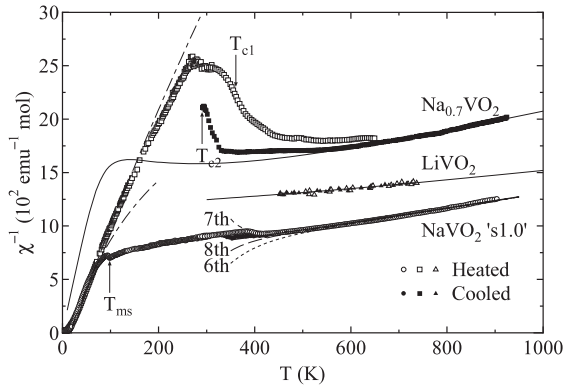

Figure 6. The temperature dependences of the magnetic susceptibilities for 's1.0' prepared from the nominal composition $NaVO_2$ and for $Na_{0.7}VO_2$ and $LiVO_2$. The dashed, short dashed and dotted curves for 's1.0' denote results calculated in terms of HTSE of up to 8th-, 7th- and 6th-order in equation (4), respectively. The full and dot–dashed curves indicate fits based on the pseudotrimer model in equation (6) and the Curie–Weiss law in equation (9), respectively. Here the calculated curves for 's1.0' consider the contribution from a small amount of $Na_{0.7}VO_2$ and all of the parameters are given in the text.

First, the results at temperatures above T_{ms} are considered. The magnetic susceptibility is expressed as a superposition of the spin term χ_d and the temperature-independent one χ_0 corresponding to the Van Vleck orbital and diamagnetic components. On the basis of the Heisenberg model

$$H = J \sum_{\langle i,j \rangle} \boldsymbol{S}_i \cdot \boldsymbol{S}_j, \tag{3}$$

where J is the exchange coupling constant, $\boldsymbol{S}$ is the spin-1 operator and $\langle i, j \rangle$ denotes a nearest-neighbour pair, the spin susceptibility of the triangular lattice in terms of the high-temperature series expansion (HTSE) of up to 8th-order is given as follows [22],

$$\chi_d^{\mathrm{HTSE}} = \frac{C}{T}\big[1 - 4(J/T) + 12.333\,33(J/T)^2 - 32(J/T)^3 + 73.842\,59(J/T)^4 - 157.9654(J/T)^5 + 322.3563(J/T)^6 - 634.2456(J/T)^7 + 1199.700(J/T)^8\big]. \tag{4}$$

Here C is the Curie constant. The dashed, short dashed and dotted curves in figure 6 denote the calculated results of up to 8th-, 7th- and 6th-order, respectively, with parameters of $C = 0.99(20)$ emu K mol^{-1}, $J = 113(30)$ K and $\chi_0 = 1.3(10)\times10^{-4}$ emu mol^{-1}, where the contribution from a small amount (10%) of $Na_{0.7}VO_2$ is taken into consideration. This C value is reasonable for V^{3+} with spin-1 and $g \simeq 2$.

Let us see how the V_3 *pseudotrimer* model explains the susceptibility data at high temperatures. A triangular cluster of three spins with the Hamiltonian

$$H = J(\boldsymbol{S}_1 \cdot \boldsymbol{S}_2 + \boldsymbol{S}_2 \cdot \boldsymbol{S}_3 + \boldsymbol{S}_3 \cdot \boldsymbol{S}_1), \tag{5}$$

is diagonalized as follows: for the total spin $S_t = 0$, 1, 2 and 3, the energy $E_{S_t} = -3J$, $-2J$, 0 and $3J$ with a degeneracy factor 1, 3, 2 and 1, respectively [3–6]. Equating the average moment per spin calculated for an isolated spin interacting with a weak applied field and an effective single-spin internal field to the average moment per spin in an exchange-coupled trimer without the next nearest-neighbour interaction [23, 24], the spin susceptibility of the pseudotrimer is given by

$$\chi_d^{\mathrm{pt}} = \frac{C}{T}\frac{1+\epsilon}{1-2\epsilon}, \tag{6}$$

and

$$\epsilon = \chi_d^{\mathrm{t}} T/C - 1, \tag{7}$$

where χ_d^{t} is the susceptibility for the local trimer given as

$$\chi_d^{\mathrm{t}} = \frac{C}{T}\frac{3p + 10p^3 + 14p^6}{1 + 9p + 10p^3 + 7p^6}, \tag{8}$$

with $p = \exp(-J/T)$. The parameters estimated in terms of HTSE lead to the full curve in figure 6. This model is found to account well for the results at high temperatures.

The pseudotrimer model is also applied to the susceptibility data for $LiVO_2$ published previously [4]. It is not easy to estimate the exchange constant with HTSE of up to 8th-order [5],

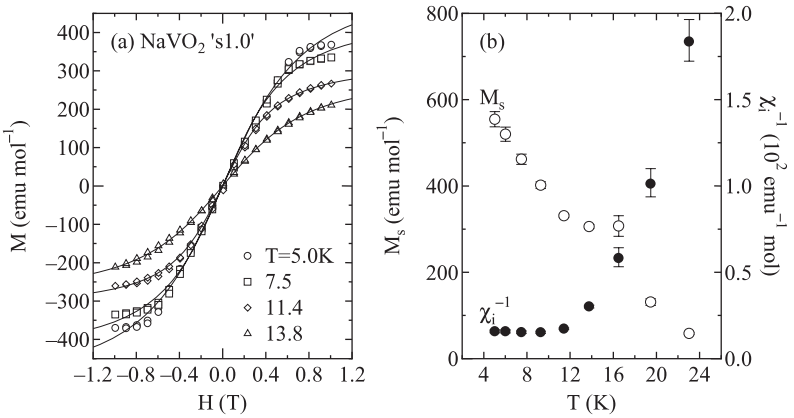

Figure 7. (a) The field dependences of magnetization for 's1.0' prepared from the nominal composition $NaVO_2$ at various temperatures, where the full curves denote fits to the Langevin function in equation (10). (b) The temperature dependences of the saturated magnetization and the inverse of initial susceptibility deduced from equation (10).

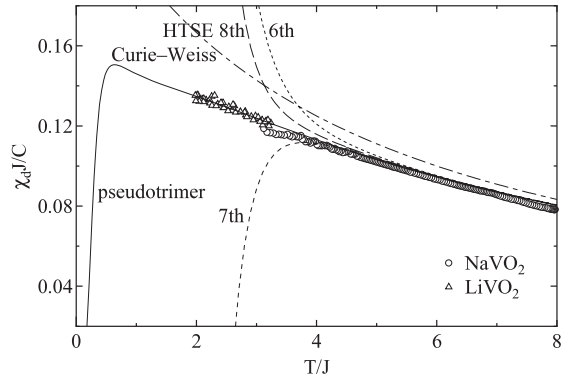

Figure 8. The reduced spin susceptibilities $\chi_d J/C$ as a function of T/J for $NaVO_2$ and $LiVO_2$. Here, the full curve indicates a fit to equation (6) of the pseudotrimer model; the dashed, short dashed and dotted curves denote results calculated in terms of HTSE of up to 8th-, 7th- and 6th-order in equation (4), respectively, and the dot–dashed curve shows the Curie–Weiss law in equation (9).

since the temperature dependence is significantly weak as compared with that of $NaVO_2$ and the data are limited below 750 K. On the other hand, the pseudotrimer model provides the reasonable fit shown by the full curve in figure 6 with the parameters of $J = 228(4)$ K and $\chi_0 = 1.7(1) \times 10^{-4}$ emu mol^{-1} for $C = 1$ emu K mol^{-1} on the assumption of $g = 2$.

It is found that the pseudotrimer model is very useful to account for the paramagnetic behaviours of the spin-1 MVO_2 system. In figure 8, the reduced spin susceptibilities defined as $\chi_d J/C$ are shown as a function of T/J based on equations (4) and (6), where the data for 's1.0' are adjusted to those per formula unit of $NaVO_2$. For comparison, the Curie–Weiss law expressed as

$$\chi_d^{CW} = C/(T + T_W), \tag{9}$$

where T_W is the Weiss temperature given as $4J$ for the spin-1 triangular lattice, is plotted by the dot–dashed curve. This law is valid only at high temperatures.

The magnetic anomaly at T_{ms} may be related to the structural transition to a tripled cell pointed out in section 3.1.1. A change or a distribution of exchange coupling constants due to the structural transition is probably responsible for the slight change of susceptibilities. At temperatures between T_{ms} and 20 K, the magnetic susceptibility apparently follows the Curie–Weiss law in equation (9) with parameters of $C = 0.070(1)$ emu K mol^{-1}, $T_W = -15.9(1)$ K and $\chi_0 = 3.2(3) \times 10^{-4}$ emu mol^{-1} as shown by the dot–dashed curve in figure 6. The Curie constant obtained here is significantly smaller than that at higher temperatures. This behaviour may be attributed to the formation of short-range ordered clusters with the superparamagnetic effect, as pointed out for the bond- and site-disordered systems of geometrically frustrated spins [25, 26]. In the present case, the uncorrelated clusters caused by the structural transition may grow against the development of spin correlation. The superparamagnetic state at low temperatures may be supported by the M–H curves with little hysteresis shown in figure 7(a). The results are empirically explained by the full curves calculated based on the Langevin function,

$$M = M_s(\coth u - 1/u), \tag{10}$$

with $u = vM_sH/T$, M_s and v being the saturated magnetization and the effective volume of the cluster, respectively. The temperature dependences of M_s and the inverse of initial susceptibility $\chi_i^{-1} = 3T/(vM_s^2)$ deduced from the $u \to 0$ limit of equation (10) are plotted in figure 7(b). M_s appears below about 25 K and its value at the lowest temperature is close to that expected from the Curie constant estimated for the temperature range between T_{ms} and 20 K. The temperature-independent behaviour of χ_i below 12 K may correspond to the blocking phenomena of spins. That is, due to the reduction of v at low temperatures, it may become difficult to turn the spin direction.

Another possible origin for the M–H curves shown in figure 7(a) would be a canted antiferromagnetism through an antisymmetric interaction in the distorted structure. However, this model usually gives rise to field hysteresis [27], which is not the case.

3.3.2. $Na_{0.7}VO_2$. The raw data for 's0.7' show a small trace of V_2O_3 as expected from the x-ray analysis; that is the jump of susceptibility that exists at about 150 K. By measuring the susceptibilities of V_2O_3 prepared according to the procedure [28] and assuming the jump of susceptibility to come from V_2O_3 alone, the data are adjusted to those per formula unit of $Na_{0.7}VO_2$ and their temperature variation is plotted in figure 6. Here, the relative amount of V_2O_3 is about 8%, which is nearly equal to that estimated from the x-ray analysis. With decreasing temperature from the high-temperature side, the susceptibility increases, and between 300 and 500 K, a first-order transition accompanied with a partial suppression, $\Delta\chi \simeq 1.9 \times 10^{-4}$ emu mol^{-1}, takes place. The width for the transition temperature is very wide, so that T_{c1} and T_{c2} are defined as the temperatures at which the susceptibility indicates a midpoint for the high- and low-temperature phases; $T_{c1(c2)} \approx 360$ (290) K. At the lower temperatures, the susceptibility increases significantly on cooling *without any anomaly*.

For $x \approx 0.7$, which is expected to have the average valence $V^{(4-x)+}$ from the ionic state of xV^{3+} and $(1-x)V^{4+}$, the local triangular cluster with two $S = 1$ and one $S = \frac{1}{2}$ is considered approximately. In this case, for the total spin $S_t = \frac{1}{2}$, $\frac{3}{2}$ and $\frac{5}{2}$, the energy $E_{S_t} = -2J$, $-\frac{J}{2}$ and $2J$ with degeneracy factors 2, 2 and 1, respectively [6]. Thus, the ground state of the local trimer is spin-$\frac{1}{2}$ and the spin susceptibility is written as

$$\chi_d^{t'} = \frac{3}{19}\frac{C}{T}\frac{2 + 20p^{3/2} + 35p^4}{2 + 4p^{3/2} + 3p^4}. \tag{11}$$

Using equations (6) and (11), the data for $Na_{0.7}VO_2$ at high temperatures are almost fitted as shown in figure 6, where the parameters are $J = 229(1)$ K and $\chi_0 = 4.1(1) \times 10^{-5}$ emu mol^{-1} for the average Curie constant $C = 0.794$ emu K mol^{-1} expected from the chemical formula on the assumption of $g = 2$. Thus, the pseudotrimer model may be valid.

The partial suppression of the susceptibility for $x \approx 0.7$ is probably attributed to the spin-$\frac{1}{2}$ trimerization accompanied by the enhancement of the exchange constant. At low

temperatures with $T \leqslant J$, the local trimers without the constant coupling between them are basically responsible for the magnetic properties and equation (11) should be applied. This leads to the Curie-type spin susceptibility, $\chi_{\rm d}^{t'} \approx \frac{3}{19}\frac{C}{T} \simeq 0.12/T$. In effect, the susceptibility data at low temperatures provide the Curie–Weiss-type form in equation (9), where $C = 0.0801(2)$ emu K mol^{-1} and $T_{\rm W} = -16.6(1)$ K using the same χ_0 as that estimated at high temperatures, as shown by the dot–dashed curve in figure 6. This is roughly consistent with the spin-$\frac{1}{2}$ trimerization model except for the superparamagnetic effect revealed for $x = 1$. Alternatively, the state of the singlet V^{3+}–V^{3+} dimer and the exchange-released V^{4+} ion or the state made up by the singlet V^{3+} trimer and the exchange-released V^{4+} cluster would give a similar behaviour for the susceptibility. The difference between the former dimer model and the spin-$\frac{1}{2}$ trimer is attributed to the exchange coupling constants within the triangular cluster. However, the latter idea is not realistic, since a significant change in the valence distribution is required. In order to confirm whether or not the spin-$\frac{1}{2}$ trimer model is appropriate for this composition, it is necessary to know details of the superlattice structure and microscopic information for the excited states.

4. Conclusions

The structural and electronic properties for specimens prepared from the nominal composition $NaVO_2$ and $Na_{0.7}VO_2$ are investigated. Both of the specimens contain minor phases, but definite conclusions for the Na_xVO_2 system are obtained through precise and systematic analyses.

$NaVO_2$ at 293 K has three oxygen layers with an octahedral coordination for Na or the O3 structure, and it is a correlated insulator with an apparent gap of 3.6×10^3 K. The paramagnetic properties at temperatures above $T_{\rm ms} \simeq 98$ K are explained in terms of the pseudotrimer model using the exchange coupling constant determined from HTSE. This analysis is also applied to the results of $LiVO_2$, and the precise exchange coupling constant is obtained. The magnetic anomaly with a slight change of susceptibility and the structural transition with the $(\frac{1}{3}\ \frac{1}{3}\ 0)$ superlattice take place at $T_{\rm ms}$. The short-range ordered cluster or the superparamagnetic state appears at the lower temperatures. That is, $NaVO_2$ does not show the spin-singlet transition, which is significantly different from the property of $LiVO_2$ with the singlet trimerization.

$Na_{0.7}VO_2$ at 293 K has two oxygen layers with a trigonal prismatic surrounding for the partially occupied Na site or the P2 structure, and it is less insulating than the case of $NaVO_2$. First-order trimerization with a spin-$\frac{1}{2}$ ground state may occur at $T_{\rm c1} \approx 360$ K on heating and $T_{\rm c2} \approx 290$ K on cooling. The reason why these transition temperatures revealed with the magnetization measurements are apparently higher than those for the transport properties is that the conduction may be influenced by atomic randomness.

The V–V distance ($d = 3.00$ Å) and the exchange coupling constant ($J = 113(30)$ K) in the paramagnetic state of $NaVO_2$ are much larger and smaller than those of $LiVO_2$ ($d = 2.91$ Å and $J = 228(4)$ K). $Na_{0.7}VO_2$ with an average V–V distance ($d = 2.87$ Å) close to that of $LiVO_2$ has $J = 229(1)$ K. Therefore, in the present system, direct exchange coupling is expected to be most effective as in the case of the V spinels [29]. Let us consider the reason why $NaVO_2$ does not exhibit the spin-singlet trimerization. J of $NaVO_2$ is smaller than that of $LiVO_2$, so that $T_{\rm c1(2)}$ is expected to be lowered. In this sense, the magnetic and structural transitions at $T_{\rm ms}$ for $NaVO_2$ might be related to the onset of spin-singlet trimerization. However, an enhancement of J with the reduction of d similar to an exchange striction in antiferromagnetic lattices may not occur due to a large ionic radius of Na or a structural suppression. Alternatively, the superparamagnetic state appears below $T_{\rm ms}$. Thus, there exists a competition between the spin-singlet state and the superparamagnetic state for the antiferromagnetically coupled spin-1 triangular lattice system. For a better understanding of this, it is necessary to estimate the gain in orbital energy due to the trimerization for $NaVO_2$.

Acknowledgments

The author thanks A Yamada and W Onoda for their help with the experiments.

References

[1] Anderson P W 1973 *Mater. Res. Bull.* **8** 153
[2] Fazekas P and Anderson P W 1974 *Phil. Mag.* **30** 423
[3] See for review Onoda M and Nagasawa H 1994 *Butsuri (Bull. Phys. Soc. Japan)* **49** 559 (in Japanese)
[4] Onoda M, Naka T and Nagasawa H 1991 *J. Phys. Soc. Japan* **60** 2550
[5] Onoda M and Inabe T 1993 *J. Phys. Soc. Japan* **62** 2216
[6] Naka T, Onoda M and Nagasawa H 1993 *Solid State Commun.* **87** 679
[7] Takada K, Sakurai H, Takayama-Muromachi E, Izumi F, Dilanian R A and Sasaki T 2003 *Nature* **422** 53
[8] Terasaki I, Sasago Y and Uchinokura K 1997 *Phys. Rev.* B **56** R12685
[9] Nakatsuji S, Nambu Y, Tonomura H, Sakai O, Jonas S, Broholm C, Tsunetsugu H, Qiu Y and Maeno Y 2005 *Science* **309** 1697
[10] See, for example Hewston T A and Chamberland B L 1987 *J. Phys. Chem. Solids* **48** 97 and references therein
[11] See, for example Fouassier C, Matejka G, Reau J-M and Hagenmuller P 1973 *J. Solid State Chem.* **6** 532
[12] Pen H F, Tjeng L H, Pellegrin E, de Groot M F, Sawatzky G A, van Veenendaal M A and Chen C T 1997 *Phys. Rev.* B **55** 15500 and references therein
[13] Chamberland B L and Porter S K 1988 *J. Solid State Chem.* **73** 398
[14] Petricek V, Dusek M and Palatinus L 2000 *Jana2000 The Crystallographic Computing System* (Praha: Institute of Physics)
[15] Shannon R D 1976 *Acta Crystallogr.* A **32** 751
[16] Zachariasen W H 1978 *J. Less-Common Met.* **62** 1
[17] See, for example Rozier P, Ratuszna A and Galy J 2002 *Z. Anorg. Allg. Chem.* **628** 1236
[18] Onoda M and Ikeda T 2007 *J. Phys.: Condens. Matter* **19** 186213
[19] Onoda M and Sugawara A 2008 *J. Phys.: Condens. Matter* submitted
[20] Onoda M 2004 *J. Phys.: Condens. Matter* **16** 8957

[21] Onoda M and Mizuguchi Y 2007 *Meeting Abstracts Phys. Soc. Japan* **62** (1) 450 (in Japanese)
[22] Yamaji K and Kondo J 1973 *J. Phys. Soc. Japan* **35** 25
[23] García-Adeva A J and Huber D L 2002 *Physica* B **320** 18 and references therein
[24] Onoda M and Hasegawa J 2003 *J. Phys.: Condens. Matter* **15** L95
[25] Mamiya H and Onoda M 1995 *Solid State Commun.* **95** 217
[26] Onoda M, Imai H, Amako Y and Nagasawa H 1997 *Phys. Rev.* B **56** 3760
[27] See, for example Onoda M and Yasumoto M 1997 *J. Phys.: Condens. Matter* **9** 3861
[28] Onoda M, Ohta H and Nagasawa H 1991 *Solid State Commun.* **79** 281
[29] Nishiguchi N and Onoda M 2002 *J. Phys.: Condens. Matter* **14** L551